Fatigue Crack Propagation Influenced by Laser Shock Peening Introduced Residual Stress Fields in Aluminium Specimens

Sören Keller[1]([✉]), Manfred Horstmann[1], Nikolai Kashaev[1], and Benjamin Klusemann[1,2]

[1] Institute of Materials Research, Materials Mechanics, Helmholtz-Zentrum Geesthacht, Max-Planck-Straße 1, 21502 Geesthacht, Germany
soeren.keller@hzg.de

[2] Institute of Product and Process Innovation, Leuphana University of Lüneburg, Universitätsallee 1, 21335 Lüneburg, Germany

Abstract. Laser Shock Peening (LSP) enables the generation and modification of residual stresses deep below the surface of metallic components. LSP-induced residual stress profiles provide penetration depths of compressive residual stresses in mm range, which can be used to retard the fatigue crack propagation (FCP) within thin sheets. These compressive residual stresses may lead to crack closure at significant applied tensile loads. This crack closure phenomenon is assumed to be one of the dominant mechanisms to reduce the load range at the crack tip, resulting in a fatigue crack retardation. This work provides an experimental and numerical investigation of the FCP in AA6056 based on C(T) 100 specimens. Residual stresses were introduced by two-sided LSP treatment of the sheet material. The resulting residual stresses were determined by the incremental hole drilling method with electronic speckle pattern interferometry. The residual stress measurements on both sides of the specimens reveal differences of the residual stresses due to the laser shock peening process design. The occurrence of crack closure was evaluated by crack opening displacement vs. load curves, which can be used to determine the crack opening force. A multi-step simulation is applied to predict the residual stress field, the stress intensity factor range and rate if residual and applied stresses are present simultaneously as well as the FCP rate. Numerical predictions and measurements of the FCP rates are in excellent agreement.

Keywords: Laser shock peening · Residual stress · Fatigue crack growth · Crack closure · Aluminium alloy

1 Introduction

To reduce structure's weight, a damage tolerant design finds application for lightweight structures (Pacchione and Telgkamp 2006), such as the fuselage of an aircraft. A damage tolerant design considers initiation and growth of cracks during the lifetime of the structure. Hence, although damages are present, the structure is in service and

able to carry the required loads. The damage of structures due to load cycles below the maximum allowable loads is named fatigue. In particular, fatigue is one of the main failure causes in the aircraft industry (Reid 2003). Laser shock peening (LSP) is a local modification technique, which can be used to extend the lifetime by introducing high compressive residual stresses. At the same time, LSP is easy to apply in industrial manufacturing processes, as it involves only the radiation of the metallic component with a pulsed laser. Clauer and Lahrman (2001) provided an overview about the achievable enhancements by LSP for different aluminium alloys.

The investigated aluminium alloy AA6056 in this study was originally developed to replace the alloy AA2024 (Blanc et al. 1998) in the aircraft industry. The aim of the developed AA6056 was the improvement of the weldability compared to AA2024. At the same time, the mechanical material behaviour and the corrosion properties of AA6056 are comparable to AA2024 (Polmear 2005; Schmidt et al. 1999). However, the yield strength of AA6056-T4 is slightly lower compared to AA2024-T351 (Amancio-Filho et al. 2008).

The application of LSP can lead to an extended lifetime of the structure/material of interest, by introducing compressive residual stresses (Kashaev et al. 2018). However, the introduced beneficial compressive stresses are balanced by tensile stresses, which in contrast might accelerate the fatigue crack propagation (FCP). The physical mechanisms (e.g. crack closure, redistribution of residual stresses, etc.) behind the fatigue crack retardation or acceleration caused by LSP-generated residual stresses are not exactly known but of high interest for an efficient application of LSP.

This study provides a combined experimental-numerical investigation of the influence of LSP on the FCP behaviour of AA6056-T4. For this purpose, first double sided LSP was experimentally applied and numerical simulated using constant LSP process parameters. Afterwards, the introduced residual stresses were measured by the incremental hole drilling method with electronic speckle pattern interferometry (ESPI). The measured residual stresses were compared to the numerically predicted residual stresses. The FCP behaviour was measured and simulated on basis of C(T)100 specimens (5 mm thickness) and subsequently interpreted in terms of the introduced residual stresses and the actual stress intensity factors. Crack opening displacement (COD) applied load curves are used to observe the change in structural stiffness of the C(T)100 specimens during the load cycles to evaluate crack closure effects.

2 Experimental Techniques and Set-up

Laser Shock Peening. Laser Shock Peening (LSP) is a local modification technique, which can be used to locally introduce compressive residual stresses into metallic components. The LSP process is schematically illustrated in Fig. 1(a). High-energy short-time laser pulses are used to vaporize the metallic surface. The vaporized material is turned into plasma, which comes along with the massive rise in temperature. The heat expansion of the material driven by the rise in temperature, causes pressure loading acting at the surface of the solid material (Fabbro et al. 1990). This surface pressure induces a shock wave, which travels through the specimen and generates
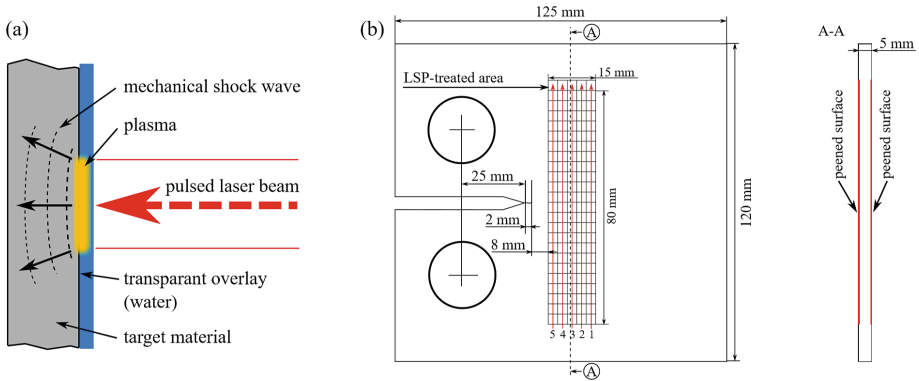
Fig. 1. (a) Schematic of the LSP process. (b) Drawing of the used C(T)100 specimens with the applied laser pulse pattern. Both sides of the C(T)100 specimens are treated twice.

plastic deformations within the material. The elastic distortion of the plastically deformed material lead to compressive residual stresses.

LSP-induced residual stresses show a characteristic profile over the depth. Compressive residual stresses, which are generated at a certain depth but still near to the surface, are balanced by tensile stresses in the centre region of the specimen, see e.g. Keller et al. (2018). However, Ocaña et al. (2015) showed that certain one-sided LSP treatments are able to produce compressive residual stresses over the entire thickness, in particular if the specimen is thin. Compared to shot peening, LSP provides a relatively high penetration depth of the resulting compressive residual stresses in addition to a high surface quality (Peyre et al. 1996).

The LSP treatment in this study was carried out with an Nd:YAG laser, producing 20 ns (full width at half maximum) laser pulses. A laser pulse energy of 5 J was used. The applied laser square 3×3 mm^2 focus enables a gapless treatment of the material without overlap of the radiated area. A laminar water layer confines the induced plasma. Laser pulses are shot with a frequency of 10 Hz. This frequency ensures a laminar water film for every laser pulse, hence, each laser pulse is shot at the same LSP conditions. Additionally to the water layer, an ablative layer could be used directly above the material. This would prevent heat effects and phase transitions of the material. For instance, Ge and Xiang (2016) used thin aluminium foils as ablative layer for the two-sided LSP treatment of C(T) specimens. Peyre et al. (1998) showed, that the application of LSP without an ablative layer lead to the generation of tensile stresses at the surface for 55C1 steel. However, it is assumed, that such tensile stresses are only influencing the crack initiation but have a minor effect on the FCP behaviour. In this study, the FCP is investigated, where the fatigue crack is developed over the entire thickness. Hence, tensile residual stresses directly below the surface are assumed negligible.

Figure 1(b) shows schematically a C(T)100 specimen including the applied LSP shot pattern. This LSP shot pattern is named LSP sequence in the following. The laser pulses were shot in columns perpendicular to the introduced crack growth direction.

The peening direction of each column is kept constant. Adjacent laser shots do not have overlapping radiated areas. The position of the first laser pulse of each column varies slightly, due to problems in the synchronization of the laser and the KUKA robot, which is used for positioning the specimen in front of the fixed laser focus. To equalize this inaccuracy of the starting point of the column position in y-direction, a relatively large column size of 80 mm is used. Therefore, the edge effects, caused by the start and end position of a single peened line, are assumed negligible, due to the relatively large distance between the crack and the edges of the peened area. The LSP sequence can be shot multiple times, which is named sequence overlap. In this regard, the shown LSP sequence is repeated once after the first LSP sequence is finished (sequence overlap of two). The C(T) specimens were treated from both sides with a sequence overlap of two. After the fist side (Side 1) was peened with the sequence overlap of two, the second side (Side 2) was treated twice with the same sequence as shown in Fig. 1(b).

Incremental Hole Drilling. Incremental hole drilling with electronic speckle pattern interferometry (ESPI) is used to measure the residual stress profiles. The measurement device used in this study is PRISM and is described in detail by Ponslet and Steinzig (2003a). According to Schajer (2010) incremental hole drilling consists of the following three steps:

- Incrementally drilling a hole.
- Measurement of the surface deformations after each increment using ESPI.
- (Inverse) calculation of residual stresses using the integral method.

While the calculation of the residual stresses based on the full field analyses of the ESPI using a least square fit is describe in Ponslet and Steinzig (2003a), underlying assumptions and restrictions are summarized by Ponslet and Steinzig (2003b). The used measuring approach of residual stresses contains two important simplifications. At first, residual stresses are assumed to be constant perpendicular to the surface, but not necessarily equi-biaxial. This assumption restricts the hole drilling method to determine residual stress fields, which change only in depth direction (perpendicular to the surface). As a second simplification, the application of the integral method assumes linear-elastic material behaviour. However, Chupakhin et al. (2016) showed that high residual stresses, which are close to 60% of the yield strength of the material, lead to plastic deformations next to the hole. These plastic deformations are due to stress concentrations caused by the edges of the hole. In a subsequent study, Chupakhin et al. (2017) illustrated for LSP typical stress profiles, that the maximum residual stress can reach 80% of the yield strength of the material before a correction is required. Above 80% of the yield strength, the observed error was significant which was accounted for by an artificial neural network approach.

Figure 2 shows specimens used for residual stress measurements, which were cut out of a peened C(T)100 specimen. The edges of the specimen for residual stress measurements have a distance of approximately 10 mm to the peened area. The diameter of the used driller was 2 mm, which enables the measurement of residual stress up to 1 mm depth. The used measurement strategy assumes linear elastic material behaviour, where the Young's modulus is assumed to be E = 70 GPa and the Poisson's
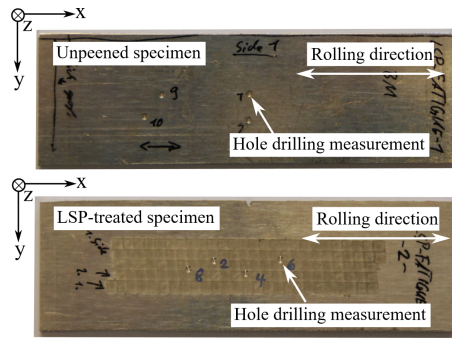
Fig. 2. Unpeened and peened (LSP-treated) specimens used for the residual stress measurements via the incremental hole drilling technique. For each process conditions, eight measurements were performed to obtain sufficient statistics.

ratio $\nu = 0.33$. According to Amancio-Filho et al. (2008), the yield strength of AA6056-T4 is $R_{p0.2} = 224$ MPa.

Fatigue Crack Propagation. FCP tests were performed according to ASTM E647-11 standard. C(T)100 specimens with a width of 100 mm are used to measure the FCP rate using the servo hydraulically testing machine from Schenk/Instron and a 25 kN load cell. Based on the ASTM standard, the change of the stress intensity factor range ΔK of unpeened specimens can be calculated using

$$\Delta K = \frac{\Delta F \cdot [2 + \alpha]}{b \cdot \sqrt{W} \cdot [1 - \alpha]^{\frac{3}{2}}} \cdot \left[0.886 + 4.64 \cdot \alpha - 13.32 \cdot \alpha^2 + 14.72 \cdot \alpha^3 - 5.6 \cdot \alpha^4 \right], \quad (1)$$

where $\Delta F = 3.78$ kN is the load alternation, $b = 5$ mm the thickness of the specimen, $W = 100$ mm the specimen width and $\alpha = a/W$ represents the ratio of the actual crack length a and width W. The specimen thickness of 5 mm prevents the specimen from buckling, which might occur otherwise at compressive external loads.

At first, specimens were pre-cracked (2 mm) to initiate a fatigue crack at the initial notch. Secondly, LSP was applied after the pre-cracking in a distance of 8 mm in front of the crack tip, see Fig. 1(b). In this work, FCP tests were conducted with two applied load ratios R_{Load} with constant amplitudes. $R_{Load} = 0.1$ is applied with the minimum force $F_{min} = 0.42$ kN and the maximum force of $F_{max} = 4.2$ kN. $R_{Load} = 0.5$ is conducted with the minimum force $F_{min} = 3.8$ kN and the maximum force of $F_{max} = 7.6$ kN. All experiments are performed at room temperature with 5 Hz. Peened specimens were tested with $R_{Load} = 0.1$ conditions only. Optical microscopes were used to measure the crack length at both sides of the specimen. The average value of the measurements from both sides is taken as the actual crack length. The peened specimens were polished in the area of the crack path to facilitate the optical measurement of the crack tip. Preliminary experiments indicated no measurable influence of the polishing on the residual stresses.

The crack opening displacement (COD) was measured at the crack mouth of the initial notch using a COD clip. A screw fixed the position of the COD clip at the specimen. The rate of the COD applied load curves corresponds to the structural stiffness of the specimen. This stiffness depends on the material stiffness (Young's modulus), the geometry of the un-cracked specimen as well as the crack length. The structural stiffness decreases with increasing crack length. The structural stiffness increases for compressive loads up to the structural stiffness of the un-cracked specimen. This recovery in stiffness is assumed to be caused by the closure of the crack (crack closure effect). Therefore, the structural stiffness of any crack length corresponds to the un-cracked specimen, in case of a completely closed crack. The highest load, at which the structural stiffness changes is named crack opening force F_{op}, because this or a higher load guarantees a completely opened crack.

3   Numerical Modelling

Multi-step Simulation Strategy. The applied multi-step simulation, as proposed by Keller et al. (2019), consist of four steps, illustrated in Fig. 3: (i) LSP process simulation; (ii) plastic strain transfer from the LSP process model to the model of the C(T) 100 specimen; (iii) prediction of the residual stresses in the C(T)100 specimen and calculation of the stress intensity factors at different crack lengths and loads; (iv) prediction of the FCP rate based on the NASGRO Eq. This multi-step simulation strategy is successfully applied to AA2024 by Keller et al. (2019). In the following, each step of the multi-step simulation strategy is shortly explained.
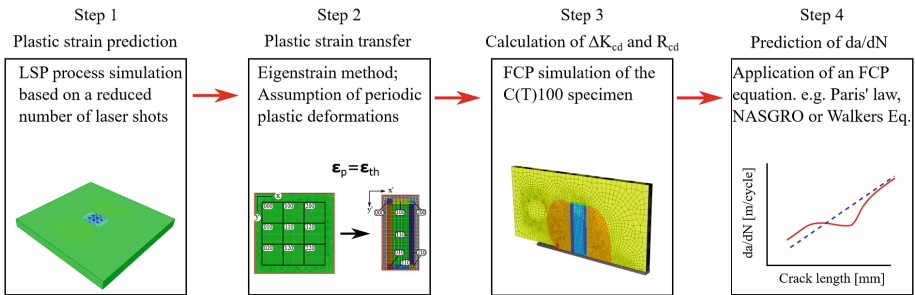

Fig. 3. Multi-step simulation strategy to predict the FCP rate. Figure reprinted from Keller et al. (2019), under the terms of the Creative Commons Attribution-NonCommercial-NoDerivatives 4.0 International (CC BY-NC-ND 4.0).

(i) The LSP process simulation predicts the plastic strains in a representative volume of the material. The representative volume is determined by the periodicity assumption of plastic strain. Accordingly to Keller et al. (2018), a square of 3×3 laser pulses, leading to an LSP-treated square of 9×9 mm^2, is found to be enough to fulfil the periodicity assumption. The plasma pressure is applied at the material surface for every laser impact, which has to be simulated. Successively, the shock wave propagates

though the material causing strain rates up to 10^6 s^{-1}. Abaqus/Explicit is used to simulate the dynamic shockwave propagation. The time between each applied laser pulse is 75 μs to guarantee a stress state that is sufficiently close to the equilibrium, as the simulation of the real frequency 10 Hz is impractical due to the numerical effort. The modelled material geometry is a $60 \times 60 \times 5$ mm^3 rectangular cuboid with fixed boundary conditions at the borders but a free top and bottom surface. Three-dimensional continuum elements C3D8R are used, where the element size at the material surface is $0.075 \times 0.075 \times 0.02$ mm^3 to guarantee a mesh independent solution. The LSP process simulation contains two main challenges: the first is the material modelling at high strain rates up to 10^6 s^{-1} and the second is the application of the correct plasma pressure at the material surface. In this work, a reduced Johnson-Cook material model, neglecting the temperature dependency, is used to consider the strain rate dependency of the yield stress σ_Y:

$$\sigma_Y = \left[A + B\varepsilon_P^n\right]\left[1 + C \ln\left[\frac{\dot{\varepsilon}_P}{\dot{\varepsilon}_{P,0}}\right]\right]. \tag{2}$$

A, B and n are material parameters describing the yield stress and its dependency on the plastic strain ε_P. The influence of the plastic strain rate $\dot{\varepsilon}_P$ is considered by the constant C and the fraction $\dot{\varepsilon}_P/\dot{\varepsilon}_{P,0}$, where $\dot{\varepsilon}_{P,0}$ is the reference strain rate that is used to determine A, B and n. The material parameters are assumed as $A = 224$ MPa, $B = 1638$ MPa and $n = 1$, simulating a linear work hardening between $R_{p0.2} = 224$ MPa and $R_m = 344$ MPa as given by Amancio-Filho et al. (2008). $\dot{\varepsilon}_{P,0}$ is assumed to be 0.0002 s^{-1}. Further material parameters of the FE simulation are the Young's modulus E = 70 GPa, the Poisson's ratio ν = 0.33, and the density $\rho = 2.8$ g/cm^3. In Keller et al. (2018), the pressure pulse was adjusted based on the resulting residual stresses in AA2198 (maximum pressure: 1350 MPa; pressure pulse duration: 200 ns), where the parameter C was taken from the literature. This adjustment corrects inaccuracies of the material modelling at high strain rate, as C cannot be experimentally determined for the present strain rate of approximately 10^6 s^{-1}. However, the adjusted pressure pulse gave precise residual stress predictions for AA2198T3-T8 and AA2024-T3 as well as for different laser shot patterns. The consequences of the material modelling approach and the chosen pressure pulse are discussed in the result section.

(ii) The LSP process simulation provides the plastic strain field within a representative volume of LSP shots. The representative volume is partitioned into small volumes, with a size of $3 \times 3 \times 0.02$ mm^3, in which the plastic strains are averaged. Afterwards, these averaged plastic strains are transferred to the model of the C(T)100 specimen as thermal strains. The area in which the thermal strains are applied corresponds to the peened area of the C(T)100 specimen (15×80 mm^2). Hence, the effect of the LSP treatment is extrapolated from the LSP process simulation (9×9 mm^2) to the much larger area of the C(T)100 specimen. As more than 500 laser pulses are applied during the two-sided LSP treatment of the C(T)100 specimen, the application of the periodicity assumption is a massive reduction of the computational effort.

(iii) Half of the C(T)100 specimen is modelled based on its symmetry. The FE model is solved in Abaqus/Standard and discretized via continuum elements (C3D8R)

of $1 \times 1 \times 0.02$ mm^3 size. A linear elastic material behaviour is assumed with the material parameters mentioned in (i). After the thermal strains are applied to the model of the C(T)100 specimen, the resulting equilibrium without external loading is calculated. The resulting stresses are the predicted residual stresses of the C(T)100 specimen. After the residual stresses are calculated, the symmetry conditions at the nodes are replaced by contact conditions to a rigid plate located at the symmetry line. The contact to the rigid plate simulates crack face contact in case of crack closure effects. The substitution of the symmetry condition is performed for every crack length at which the stress intensity factors are calculated. The stress intensity factor is calculated for the minimum and maximum applied load using the crack closure technique (Krueger 2004). Related to its impact on the FCP, the calculated stress intensity factor is named crack driving stress intensity factor K_{cd}. Plane stress conditions are assumed.

(iv) The crack driving stress intensity factor range $\Delta K_{cd} := K_{cd}(F_{max}) - K_{cd}(F_{min})$ and ratio $R_{cd} := K_{cd}(F_{min})/K_{cd}(F_{max})$ are used as input for the reduced, neglecting fracture toughness and threshold regime, NASGRO equation (NASGRO® Consortium, 2001)

$$\frac{da}{dN} = C_{NA}\left[\Delta K_{cd}\frac{[1-f_N]}{[1-R_{cd}]}\right]^{n_{NA}}. \tag{3}$$

$C_{NA} = 1.016e^{-9}$ and $n_{NA} = 2.21$ in the NASGRO equation were identified in this contribution by FCP experiments of the untreated material, see Fig. 6. f_N is the crack opening function found by Newmann (1984). Accordingly, to (iii) plane stress conditions are assumed.

4   Results and Discussion

Residual Stress Measurements. The results of the residual stress measurement of the unpeened (BM) and peened (LSP) specimens are illustrated in Fig. 4. The residual stresses were measured from both sides with a maximum measuring depth of 1 mm. Side 1 was peened at first with an LSP sequence overlap of two; afterwards Side 2 was peened in the same way. The z-coordinate, describing the depth direction of the specimen, starts at $z = 0$ mm at the surface of Side 1 and ends at $z = 5$ mm at the surface of Side 2.

Both sides show significant changes of the residual stress fields after LSP treatment (σ_{LSP}) compared to the unpeened material (σ_{BM}). The fabrication process of the specimens like rolling and cutting may cause initial residual stresses. However, this effect is similar for both sides, results from hole drilling of the unpeened material are averaged from the measurements of both sides at each specific depth. The low standard deviation of the measurements indicate that the residual stresses of the unpeened material do not depend on the side as expected.

The LSP treatment introduces significant compressive residual stresses with a penetration depth more than 1 mm below the surface. The penetration depth might be even further optimized; however, the used laser pulse and sequence parameters lead to
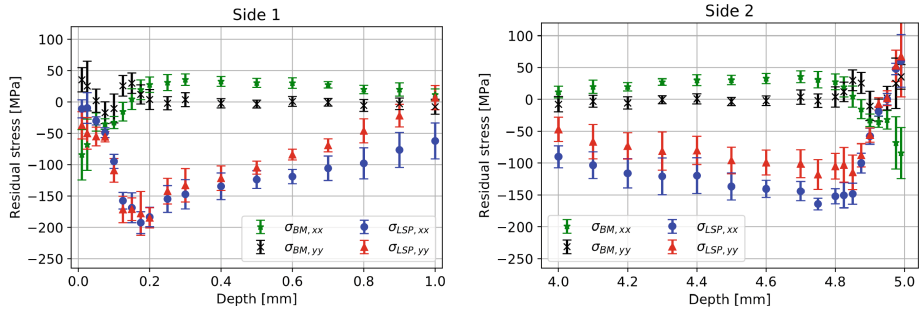
Fig. 4. Mean value and standard deviation of the measured residual stresses of Side 1 and Side 2 for peened (σ_{LSP}) and unpeened (σ_{BM}) specimens next to the surfaces at 0 mm and 5 mm. Both, Side 1 and 2 show comparable compressive residual stresses, however, differences in terms of penetration depth and the tensile stresses next to the surface at Side 2 are indicated.

clearly measureable effects of the LSP treatment on the FCP rate, which makes the introduced residual stresses sufficient for this study.

Side 1 indicates compressive residual stresses over the entire measured depth. In contrast, Side 2 shows tensile residual stresses at the surface, which turns into compressive residual stresses after a depth of 0.05 mm. Tensile stresses directly at the surface were measured during other experiments without an ablative layer as well, see Peyre et al. (1998) and Keller et al. (2018). Therefore, the authors conclude that the LSP treatment of Side 2 turned initial tensile stresses at the surface of Side 1 into compressive stresses. Additionally, residual stresses at Side 1 show higher maximum compressive residual stresses compared to Side 2. However, residual stresses at Side 2 decrease slower with depth, hence, a higher penetration depth of compressive residual stresses is observed. This observation show that the depth at which residual stresses are influenced by a certain laser pulse sequence depends strongly on the initial residual stress field present in the specimen before LSP.

Both sides indicate a nearly equi-biaxial residual stress field directly below the surface. At a certain depth differences of the residual stresses depending on the stress direction ($\sigma_{xx} \neq \sigma_{yy}$) occur. This observation fits into the non equi-biaxial residual stresses for a high-energy input as reported for AA2198 (Keller et al. 2018).

Residual Stress Calculation and Adjustment of the Strain Rate Dependency Parameter. Residual stresses are predicted in (iii) of the multi-step simulation strategy. As described, the material modelling at high strain rates (not precisely known material behaviour at high strain rate) and the application of the correct pressure pulse (connection laser to resulting pressure pulse not precisely known) are main challenges of the LSP process simulation. To obtain suitable results, either the pressure pulse or the material properties can be adjusted. In Keller et al. (2018), the material properties are assumed to be known from the literature and the resulting plasma pressure, acting at the material surface is adjusted to fit the measured residual stresses. This adjustment included three different parameters for the time dependency of the pressure pulse. The plasma pressure was simplified, as the experimental spatial distribution of the used Nd:

YAG laser is constant. Based on the assumption of the hole drilling method, measured residual stresses can be interpreted as an average stress of the local stresses located in a plane parallel to the surface around the drilled hole. Therefore, the numerically predicted residual stresses were averaged in a representative area parallel to the surface plane as well. This averaging does not allow the experimental validation of local residual stress gradients perpendicular to the depth direction, which would otherwise also lead to an assumption of a constant spatial distribution of the pressure pulse. Hence, the adjusted pressure pulse is not necessarily the physically correct plasma pressure, as for instance the averaging scheme of the predicted residual stress field might lead to same results of different applied pressure pulses. In addition, this adjustment neglects inaccuracies of the not precisely known material behaviour at high strain rates. Because of our promising application to the AA2xxx series (Keller et al. 2018, 2019), the identified pressure pulse is used for the AA6xxx series in this work as well. The assumption, that the adjusted pressure pulse has the same physical effect on the material than the real plasma pressure, allows adjusting the material (strain-rate) dependency to match the measured residual stresses in AA6056. Assuming, the Johnson-Cook material model is sufficient to cover the strain rate effect, and taking $\dot{\varepsilon}_{P,0}$ as constant and known, only the material parameter C has to be fitted.

Figure 5 illustrates the effect of C on the resulting residual stresses. As C scales the yield stress, a lower value of C reduces the resistance to high strain rates, leading to plastic deformations of the material at a lower magnitude of the mechanical shock wave. Consequently, this leads to higher penetration depth of plastic deformations and, therefore, residual stresses as well. The larger influencing depth of the shock wave for a lower value of C is also indicated by the drop of the residual stresses at 1 mm depth for $C = 0.01$. This drop of the residual stresses is interpreted as an interaction of residual stresses on Side 1 (surface at 0 mm) and the shock waves initiated at Side 2 (surface at 5 mm). This interaction is not visible in the residual stress profile for $C = 0.1$. Difference of the residual stress component in x-axis direction σ_{xx} and in y-axis direction σ_{yy}, described as non equi-biaxiality increases with a lower value of C. As shown in Fig. 5, the measured and predicted residual stresses are in a good agreement for taking $C = 0.07$.
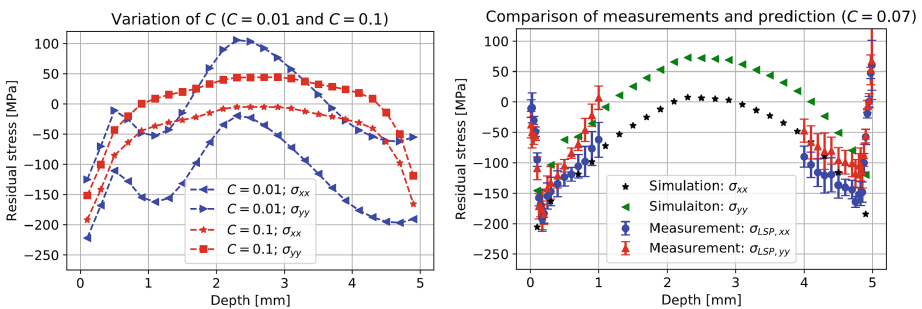

Fig. 5. Influence of the strain rate dependency parameter on the predicted residual stress distribution and comparison between measured and predicted residual stresses. The strain rate dependency parameter $C = 0.07$ was adjusted considering the measured residual stresses.

Fatigue Crack Propagation. Measured and predicted fatigue crack propagation rates depending on the crack length are in a good agreement for both unpeened and peened specimens, see Fig. 6. While the stress intensity factor prediction of peened specimens is based on the multi-step simulation, Eq. (1) is used to predict the stress intensity factor range and rate for the unpeened specimen. The LSP treatment lead to an increased FCP rate between the initial crack tip and the peened area. This area contains typically tensile residual stresses, balancing the compressive residual stresses introduced by LSP. Tensile residual stresses lead to an increased stress intensity factor ratio but an unchanged stress intensity factor range, as predicted by the numerical results. The unchanged stress intensity factor range indicates that the influence of the residual stresses on the minimum and maximum stress intensity factor is the same, which corresponds to traditionally used superposition principles, see Parker (1982) or Itoh et al. (1989). As the stress intensity factor range remains unchanged, the acceleration of the FCP is caused by the increased stress intensity factor ratio. Therefore, FCP equations that should be applied to the region in front of the peened area have to consider the influence of the stress intensity factor ratio. In particular, Paris' law is not sufficient to predict the FCP rate up to the length of 35 mm. This conclusion is drawn and illustrated by Keller et al. (2019).

The stress intensity factor range, ratio, and the FCP rate decrease after the crack reached the peened area at 35 mm. The FCP rate of the peened specimen drops below the FCP rate of the unpeened specimen at approximately 40 mm. Therefore, LSP treatment leads to a retardation of the FCP after one-third of the peened area, which is located at a crack length between 35 mm and 50 mm. The maximum retardation is reached at approximately 46 mm. Afterwards the FCP rate increases and finally converges to the FCP rate of the unpeened specimen. Thus, possible tensile stresses behind the peened area do not lead to a further acceleration, in contrast to the stresses in front of the peened area.

The peening at a certain distance to the crack tip led to an acceleration of the FCP rate. Therefore, peened and unpeened specimens in this study showed a similar fatigue life. The residual stresses can be optimized to extend the fatigue performance. For instance, Chupakhin et al. (2019) used design of experiments to evaluate the relation between LSP parameters and the fatigue life. A further investigation of optimal LSP treatment, in particular from a numerical perspective, will be part of future work.

Crack Opening Displacement. The observation of a deceleration of the FCP rate, which is correlated to the decreased stress intensity factor range inside and behind the peened area (35 – 60 mm) leads to the question of the responsible mechanisms. For this purpose, Fig. 7 illustrates the applied load COD curves of a C(T)100 specimen at different crack lengths, to detect crack closure effects. To record the shown applied load COD curves, the applied load cycle were changed to 1.8 kN and - 1.8 kN as maximum and minimum loads, respectively. After the applied load COD curves were recorded, the load cycle was immediately changed back to the previous test condition of 0.42 – 4.2 kN, to reduce the impact of the compressive loads on the fatigue test results to a minimum. The measurements show oscillations, which are due to the controlling system of the load in the experimental set up. However, the general trends of the applied load COD curves are clearly visible.
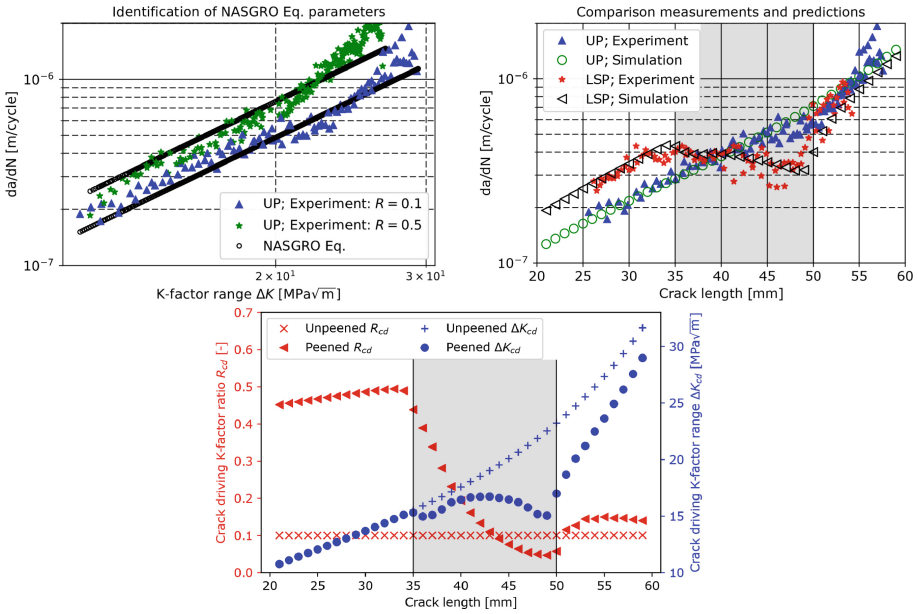
Fig. 6. FCP rate (da/dN) of the unpeened (UP) material and the predictions of the NASGRO Eq. for the identified parameters $C_{NA} = 1.016e^{-9}$ and $n_{NA} = 2.21$. Stress intensity factor ratio R_{cd} and range ΔK_{cd} influenced by the applied and residual stresses simultaneously in comparison to residual stress free samples. Grey background indicates peened area. The FCP rate depends on the crack length for unpeened and peened (LSP) specimens (two samples each). LSP treatment leads to an acceleration of the fatigue crack propagation in front of the peened area and to a retardation of the fatigue crack within the peened area.

LSP treatment influences the structural stiffness of the C(T)100 specimens significantly, as illustrated in Fig. 7. The structural stiffness of the peened specimens with a crack length of 55 mm changes slightly but continuously between approximately 0 kN and 1 kN. This indicates a higher F_{op} compared to the unpeened specimen. This increased opening load is interpreted as the result of the compressive residual stresses, which cause crack closure within the peened area. In addition, the load range in which the structural stiffness changes from the opened crack geometry to the closed crack geometry is increased as well. This increase in the load range where the structural stiffness changes indicates an opening and closing effect of the crack during the load cycles. The structural stiffness of the peened specimens at low loading forces does not correspond to the stiffness of an un-cracked specimen, which indicates a partially closed crack.

The FCP experiments indicate no significant influence of the LSP treatment behind the treated area (crack length: 50–55 mm), see Fig. 6. However, applied load-COD measurements show a significant increase of the crack opening force for the crack length of 55 mm. The occurrence of a high crack opening force without a significant crack growth retardation shows the complex mechanisms at the crack tip. Although
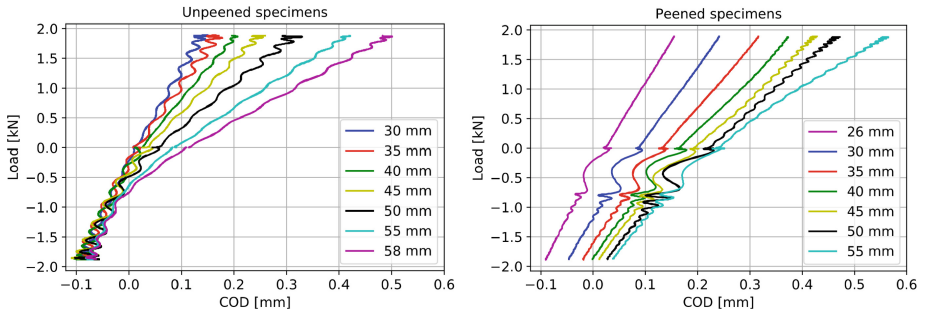
Fig. 7. Applied load-COD curves for different crack lengths of an unpeened and peened C(T) 100 specimen. The stiffness of the specimen changes with decreasing external load. The recovery of stiffness for compressive loading is caused by crack closure. The stiffness of the specimen with a closed crack corresponds to an un-cracked specimen, however, this stiffness is not reached in case of peened specimens indicating a partially opened crack.

crack closure occurs and the crack opening force is drastically increased, the stress intensity factor range is just slightly decreased. A detailed analysis of the fatigue crack retarding and accelerating mechanisms will be reported in the future.

5   Conclusion

The fatigue performance of AA6056 was modified by a two-sided LSP treatment and evaluated based on fatigue crack propagation tests and a multi-step simulation. The introduced residual stresses were measured using the incremental hole drilling technique and predicted by an LSP process simulation. The predicted residual stresses are used to predict the stress crack driving intensity factors for the peened specimen at the maximum and minimum applied loads. Parameters of the NASGRO Eq. were identified based on experiments on unpeened specimens. Afterwards, the predicted crack driving stress intensity factors are used to predict the FCP rate resulting from the NASGRO Eq. COD measurements were used to investigate the crack closure effects, which are linked to a reduced crack driving stress intensity factor range in and behind the peened area. Therefore, crack closure is assumed to be the main mechanism to retard the FCP. The main conclusions of this study can be summarized as follows:

- The multi-step simulation strategy from Keller et al. (2019) is applied to predict the FCP rate influenced by LSP-induced residual stresses in AA6056-T4.
- The order in which the sides of the AA6056 sheet were peened influences the resulting residual stresses.
- Fatigue crack propagation tests showed that the LSP treatment did not lead to an increased fatigue life in this study. The fatigue crack accelerates before the crack reaches the peened area. This acceleration is connected to tensile residual stresses in front of the peened area, which are balancing the preferred compressive residual stresses in the LSP-treated area. This highlights the importance of applying an

optimized LSP treatment based on the position of the already present cracks in the structure for repair applications.

- Significant differences of the applied load COD curves of peened and unpeened specimens are observed. These differences are linked to crack closure phenomena of the fatigue crack at low applied loads. As crack closure occurs for the same crack lengths where the stress intensity factor range is reduced, crack closure is assumed to be an important mechanism to retard the fatigue crack propagation.
- Crack closure is expected even 10 mm behind the peened area, as the applied load COD curve of the peened specimen differs from the unpeened specimen. However, the FCP is not retarded significantly. Hence, the crack opening force F_{op} cannot be used as the only input to calculate the FCP rate.

References

Amancio-Filho, S., Sheikhi, S., dos Santos, J., Bolfarini, C.: Preliminary study on the microstructure and mechanical properties of dissimilar friction stir welds in aircraft aluminium alloys 2024-T351 and 6056-T4. J. Mater. Process. Tech. **206**(1–3), 132–142 (2008)

Blanc, C., Roques, Y., Mankowski, G.: Application of phase shifting interferometric microscopy to studies of the behaviour of coarse intermetallic particles in 6056 aluminium alloy. Corros. Sci. **40**(6), 1019–1035 (1998)

Chupakhin, S., Kashaev, N., Huber, N.: Effect of elasto-plastic material behaviour on determination of residual stress profiles using the hole drilling method. J. Strain Anal. Eng. Des. **51**(8), 572–581 (2016)

Chupakhin, S., Kashaev, N., Klusemann, B., Huber, N.: Artificial neural network for correction of effects of plasticity in equibiaxial residual stress profiles measured by hole drilling. J. Strain Anal. Eng. Des. **52**(3), 137–151 (2017)

Chupakhin, S., Klusemann, B., Huber, N., Kashaev, N.: Application of design of experiments for laser shock peening process optimization. Int. J. Adv. Manuf. Technol. **102**(5–8), 1567–1581 (2019)

Clauer, A.H., Lahrman, D.: Laser shock processing as a surface enhancement process. F. Key Eng. Mater. **197**, 121–144 (2001)

Fabbro, R., Fournier, J., Ballard, P., Devaux, D., Virmont, J.: Physical study of laser-produced plasma in confined geometry. J. Appl. Phys. **68**(2), 775–784 (1990)

Ge, M.-Z., Xiang, J.-Y.: Effect of laser shock peening on microstructure and fatigue crack growth rate of AZ31B magnesium alloy. J. Alloy. Comp. **680**, 544–552 (2016)

Itoh, Y.Z., Suruga, S., Kashiwaya, H.: Prediction of fatigue crack growth rate in welding residual stress field. Eng. Fract. Mech. **33**(3), 397–407 (1989)

Kashaev, N., Chupakhin, S., Ventzke, V., Horstmann, M., Riekehr, S., Barbini, A., dos Santos, J., Keller, S., Klusemann, B., Huber, N.: Fatigue life extension of AA2024 specimens and integral structures by laser shock peening. In: MATEC Web of Conferences, vol. 165, p. 18001 (6p.) (2018)

Keller, S., Chupakhin, S., Staron, P., Maawad, E., Kashaev, N., Klusemann, B.: Experimental and numerical investigation of residual stresses in laser shock peened AA2198. J. Mater. Process. Tech. **255**, 294–307 (2018)

Keller, S., Horstmann, M., Kashaev, N., Klusemann, B.: Experimentally validated multi-step simulation strategy to predict the fatigue crack propagation rate in residual stress fields after laser shock peening. Int. J. Fatigue **124**, 265–276 (2019)

Krueger, R.: Virtual crack closure technique: history, approach, and applications. Appl. Mech. Rev. **57**, 109–143 (2004)

NASGRO® Consortium and Others: (2001). Fatigue crack growth computer program NASGRO® version 3.0. User manual. JSC-22267B. NASA Technical report

Newmann Jr., J.: A crack opening stress equation for fatigue crack growth. Int. J. Fract. **24**, R131–R135 (1984)

Ocaña, J.L., Correa, C., García-Beltrán, A., Porro, J.A., Díaz, M., Ruiz-de-Lara, L., Peral, D.: Laser shock processing of thin Al2024-T351 plates for induction of through-thickness compressive residual stresses fields. J. Mater. Process. Tech. **223**, 8–15 (2015)

Pacchione, M., Telgkamp, J.: Challenges of the metallic fuselage. In: Proceeding 25th ICAS. Hamburg, Germany (2006)

Parker, A.P.: Stress intensity factors, crack profiles, and fatigue crack growth rates in residual stress fields. In: Residual Stress Effects in Fatigue. ASTM International, Materials Park, USA (1982)

Peyre, P., Fabbro, R., Merrien, P., Lieurade, H.: Laser shock processing of aluminium alloys. Application to high cycle fatigue behaviour. Mater. Sci. Eng.: A **210**(1–2), 102–113 (1996)

Peyre, P., Berthe, L., Scherpereel, X., Fabbro, R.: Laser-shock processing of aluminium-coated 55C1 steel in water-confinement regime, characterization and application to high-cycle fatigue behaviour. J. Mater. Sci. **33**(6), 1421–1429 (1998)

Ponslet, E., Steinzig, M.: Residual stress measurement using the hole drilling method and laser speckle interferometry. Part II: Analysis technique. Exp. Tech. **27**(4), 17–21 (2003a)

Ponslet, E., Steinzig, M.: Residual stress measurement using the hole drilling method and laser speckle interferometry part III: analysis technique. Exp. Tech. **27**(5), 45–48 (2003b)

Polmear, I.: Light alloys: from traditional alloys to nanocrystals. In: Light Alloys, 4th edn. Elsevier Ltd., Amsterdam, The Netherlands (2005)

Reid, L.: Sustaining an Aging Aircraft Fleet with Practical Life Enhancement Methods. Fatigue Technology Inc., Seattle, USA (2003)

Schajer, G.S.: Advances in hole-drilling residual stress measurements. Exp. Mech. **50**(2), 159–168 (2010)

Schmidt, H.J., Schmidt-Brandecker, B., Ohrloff, N., Fleischer, T.: Current status of research and development activities for the fuselage of a large airbus aircraft. In: 20th Symposium of the ICAF, pp. 537–552. Bellevue, USA (1999)